COBEM 2023 27TH INTERNATIONAL CONGRESS OF MECHANICAL ENGINEERING

ABCM Brazilian Society of Mechanical Sciences and Engineering
27th ABCM International Congress of Mechanical Engineering
December 04-08, 2023, Florianópolis-SC, Brazil

COB-2023-1255
EFFECTS OF THICKNESS CHANGES ON THE THICKNESS ATTENUATORS FLOWS ASSOCIATED IN SERIES IN PULSED FLOWS

Gustavo Cordeiro Barreiros
Matheus Campos Vieira
Pedro Henrique Bergamim Bis
João Paulo Barbosa
Renato do Nascimento Siqueira
Ayrton Cavallini Zotelle
GPMF, Department of Mechanical Engineering, Instituto Federal do Espírito Santo - *Campus* São Mateus, Rod. BR 101 norte, km 58, Litorâneo, São Mateus - ES, 29932-540, Brazil
guicordeiro42@gmail.com
matheuscamposvieira@hotmail.com
pedrobbis@hotmail.com
jpbarbosa@ifes.edu.br
renatons@ifes.edu.br
ayrton.zotelle1@hotmail.com

Abstract. *Vibrations in pipelines are common in systems with alternative pumps due to the fluctuating and pulsating flow generated by these devices. Flow attenuators are installed to reduce these vibrations by absorbing the pressure and flow oscillations produced by the pump. The efficiency of flow attenuators can be enhanced by adjusting geometric parameters, such as thickness, and by arranging them in series. This study analyzed the behavior of series-connected flow attenuators, varying their thickness, to investigate the differences in flow fluctuation attenuation and distribution. Numerical simulations were conducted using specific software. Two geometric configurations of attenuators were considered: a straight tube and a variation consisting of sections connected in series. The thickness of the attenuators ranged from 1 to 3 mm. The results showed that the thickness of the series-connected attenuators significantly influences flow fluctuation attenuation. Thinner attenuators yielded better results. Geometric modifications and the arrangement of attenuators are decisive factors in optimizing system performance, resulting in performance improvements in process units that employ alternative pumps.*

Keywords: *Flow attenuators, series flow attenuators, Fluid-Structure Interaction, thickness, geometric modification.*

1. INTRODUCTION

Positive displacement pumps, also known as reciprocating pumps, are widely used in various industrial sectors, including refineries, petrochemical facilities, and oil platforms. However, these pumps have a peculiar characteristic that can cause unwanted disturbances in pipeline systems: the fluctuating flow with a sinusoidal pattern (Xiaohui *et al.*, 2015). This flow fluctuation occurs due to the operation of reciprocating pumps, especially axial piston pumps, which use check valves based on pressure difference, resulting in periodic discharge of fluid due to piston movement. The flow fluctuation from positive displacement pumps can generate significant vibrations in pipeline systems. To address these problems resulting from vibrations in refinery pipelines and other industrial processes, it is common to use external devices called flow attenuators or pulsation dampeners, positioned after the reciprocating pumps. These devices play an essential role in controlling the pulsations generated by the pumps, providing an effective solution to reduce pulsating pressures and flow fluctuation (Bernart, 1999). The use of a single flow attenuator may have limitations in fully absorbing the flow fluctuations generated by the pump. In this context, studies have investigated the use of multiple interconnected attenuators in series along the main line, aiming to absorb the energy of flow variations throughout the system (Xiaohui *et al.*, 2015). However, in the oil and gas industry, it is common to use a central hydraulic system to supply multiple wells with a single pump, resulting in multiple connection lines to the main line. This requires calculating the energy requirements of the main system, considering factors such as injection gas pressure, injection point depth, and pump gas flow (Viersma, 1980). In addition to the number of attenuation devices, the type of attenuator used plays a relevant role. For example, there are bladder-type attenuators that use a flexible membrane and gases to absorb the energy of flow variations, and resistive attenuators, such as in-line models, composed only of flexible elastomer tubes. While bladder-type attenuators require the presence of gas to function, resistive attenuators do not have this requirement, making them a more economically viable option and easily integrable into the pipeline system. Given the structural complexity of flow attenuators, analytical methods have limitations in analyzing these structures. As an alternative, numerical methods have been em-

ployed, allowing the simulation of the dynamic behavior and interaction between the moving fluid and the deformable structure of the attenuators. These methods provide an effective approach to evaluating the performance of attenuators under different operating conditions. In this context, the objective of this study is to analyze, using numerical tools based on fluid-structure interaction (FSI), the effect of fractional flow attenuators arranged in series. Furthermore, it aims to investigate the influence of different attenuator thicknesses on the attenuation of flow peaks generated by positive displacement pumps. Understanding the behavior of these attenuators in relation to fractionalization and thickness variation is crucial to enhance the efficiency of these devices and propose more effective solutions for reducing flow fluctuations.

2. METHODOLOGY

The fluid-structure analysis was conducted using a two-way coupling approach, employing ANSYS Fluent © for fluid analysis, ANSYS Mechanical © for structural analysis, and ANSYS System Coupling © to facilitate integration between these simulations.

2.1 Geometry and boundary conditions

The geometry of the flow attenuator was created using the Design Modeler drawing tool available in the Ansys® software package. The geometry consists of a main cylinder representing the fluid volume with a radius of r = 6.35 mm and a length of L = 600 mm. Additional cylinders were created at the ends of this cylinder to represent the rigid piping, and an internal face was added to apply the pressure drop condition. From the external surface of this main cylinder, a surface was created to represent the attenuator wall, corresponding to the structural domain, with a thickness of h = 1 mm. To save computational resources, a symmetry condition was used, as shown in Figure 3. Figure 1a represents the reference geometry used for the mesh test, and Fig. 1b is the configuration used to represent the attenuator in series by sectioning the reference geometry.

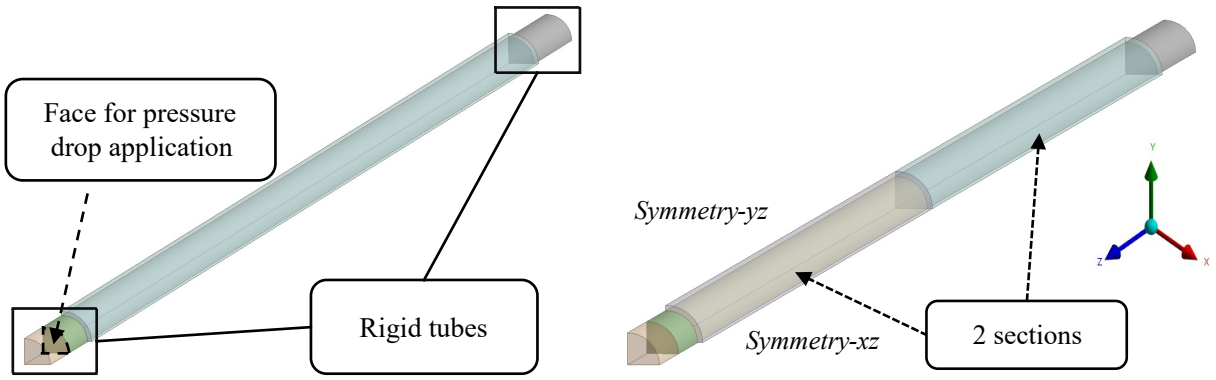

(a) Reference. (b) Sectioned.

Figure 1: Geometries used in the simulations.

In the structural domain, the analysis was performed considering natural linear rubber, described in Shahzad *et al.* (2015) study as an incompressible, homogeneous, and isotropic material. Fixed supports were applied at the ends of the rubber attenuators as boundary conditions, and a fluid-structure exchange interface was established to ensure proper constraint and allow interaction between the structure and the surrounding fluid. In the fluid domain, boundary conditions were set to simulate the flow through the attenuator. Non-slip conditions were applied to the walls, and a porous jump was used to model flow with a pressure drop across the porous medium. At the inlet region, a transient and fully developed velocity profile was applied. This profile started with an average velocity (V_m) of 0.09494 m/s and then transitioned to a transient regime with a sinusoidal curve of amplitude 0.01187 m/s and a frequency of 1 Hz (Eq. 1). At the outlet region, a manometric pressure equal to 0 was imposed. Water was used as the fluid in the simulation, and laminar flow was considered.

$$V(t) = \begin{cases} 0.09494, & \text{if } t \leq 3 \\ 0.09494 + 0.01187 \cdot \sin(2\pi t), & \text{if } t \geq 3 \end{cases} \tag{1}$$

Equation 1 can be divided into two distinct periods. In the first period, which extends up to 3 seconds, the focus is on the gradual filling of the fluid in the attenuator, resulting in its deformation until an equilibrium is reached with the internal stresses. After 3 seconds, the pulsating flow begins.

2.2 Mathematical formulation

Fluid-structure interaction (FSI) combines structural analysis methodologies with advanced computational fluid mechanics techniques. The equations that describe the behavior of the solid structure depend on the nature of the material and the desired level of complexity in the simulation. For linear structures, the equilibrium equations can be described by the principle of conservation of linear momentum, that is, the constitutive equations are based, in this case, on Hooke's law (Sang *et al.*, 2017).

$$\rho_s \frac{\partial^2 \vec{d_s}}{\partial t^2} = \nabla \cdot \sigma_s + \vec{f_s}, \tag{2}$$

$$\sigma_s = c : \epsilon, \tag{3}$$

$$\epsilon = \frac{1}{2}\left[\left(\nabla \vec{d_s}\right) + \left(\nabla \vec{d_s}\right)^T\right], \tag{4}$$

where ρ_s is the material density, σ is the second-order stress tensor, $\vec{f_s}$ represents the external forces applied, c is the fourth-order stiffness tensor, $\vec{d_s}$ is the displacement vector, and ϵ is the strain tensor.

The equations governing fluid flow and associated phenomena are derived from the basic principles of mass conservation and momentum conservation. This leads to the governing equations of fluid flow (Versteeg and Malalasekera, 2007). For a deforming control volume, the variation of relative motion at the boundaries becomes a factor, and the rate of change of the control volume's shape becomes part of the analysis. Consequently, the mass conservation equation that describes fluid continuity for a deformable tube can be written as follows:

$$\frac{\partial \rho_f}{\partial t} + \nabla \cdot (\rho_f \vec{U}) + \frac{1}{V_m}\left[\frac{\partial}{\partial t}\int_{Vc} \rho_f \, dV(t) + \int_{Sc} \rho_f \vec{U} \cdot \vec{n} \, dA(t)\right] = 0 \tag{5}$$

where ρ_f is the fluid density, t is time, $\vec{U}$ is the velocity vector, V_m represents the average volume of fluid in the control volume, and $\vec{n}$ is the normal vector to the surface. This equation describes the variation of fluid density over time, considering convective transport and volume deformation.

As for the momentum equation, it describes the relationship between the rate of change of linear motion and the forces acting on a fluid. This equation is a direct application of Newton's second law for fluids. It considers both surface forces, such as pressure and viscous forces, and body forces, such as gravity (Hibbeler, 2016).

Therefore, considering laminar flow with constant density and viscosity, the governing equations of fluid flow can be expressed in terms of the body forces per unit volume ($\vec{f_f}$), fluid density (ρ_f), pressure (p), and dynamic viscosity (μ) (Tey *et al.*, 2017):

$$\rho_f \frac{\partial(\vec{U})}{\partial t} + \rho_f \vec{U} \cdot (\nabla \vec{U}) = -\nabla p + \mu(\nabla^2 \vec{U}) + \vec{f_f} \; . \tag{6}$$

Finally, data transfer between the fluid and the solid is established through a fluid-solid coupling, subject to two conditions that must be satisfied. The first condition is known as the kinematic condition (Wang and Yan, 2010), expressed as follows:

$$\vec{d_f} = \vec{d_s}, \tag{7}$$

where $\vec{d_f}$ and $\vec{d_s}$ represent the displacements of the fluid and the solid, respectively.

The second condition is the stress equilibrium, given by:

$$\sigma_f \vec{n} = \sigma_s \vec{n}, \tag{8}$$

where σ_f and σ_s are the stresses of the fluid and the solid, respectively. $\vec{n}$ is the unit normal vector to the fluid-structure interface.

The relationship between the structure and the fluid can be simplified as follows: the configuration of the structure affects the flow conditions at the fluid interface, resulting in changes in pressure and viscous forces. These changes, in turn, impact the motion of the structure itself. To describe the behavior of the structure, the Finite Element Method (FEM) was employed, and Finite Volume Method (FVM) was used in fluid dynamic simulations.

3. RESULTS AND DISCUSSIONS

3.1 Influence of the thickness of the flow attenuator

Figure 2 illustrates the variations in fluid inlet and outlet velocities for different attenuator thicknesses. In all simulations conducted, a reduction in the amplitude of the outlet flow was observed, and this reduction became less significant as the attenuator wall thickness increased, following a trend predicted in the literature. Additionally, in these specific cases, it was possible to identify a change in the phase of the velocity at the outlet compared to the inlet, as evidenced by the different time instances at which the velocity peaks occur (with a phase shift of 0.16 seconds), corresponding to a phase angle of 57.6°. This observed behavior can be attributed to the time required for the tube to expand and accommodate the fluid inside it.

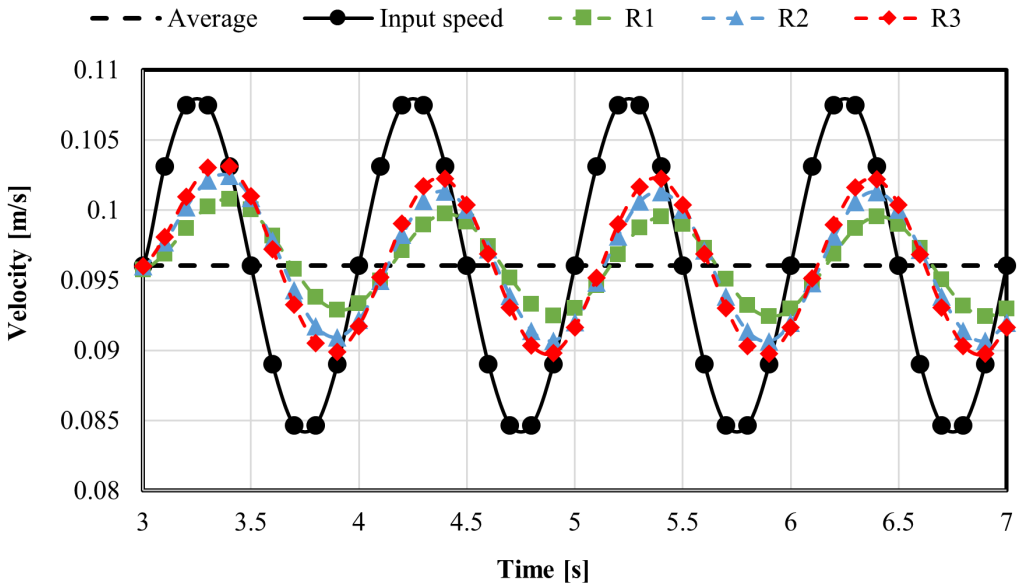

Figure 2: Comparison between the exit velocities for the reference attenuators, with R1, R2, and R3 corresponding to attenuators with thicknesses of 1 mm, 2 mm, and 3 mm, respectively.

To evaluate the performance of the attenuator, it is essential to implement the attenuation factor or simply attenuation (%A), calculated as follows:

$$\%A = \frac{Q_e(t) - Q_s(t)}{Q_e(t) - Q_m} \cdot 100. \tag{9}$$

where $Q_e(t)$ is the inlet flow rate, $Q_s(t)$ is the outlet flow rate, and Q_m is the average flow rate.

In Figure 3a, the attenuations for the three analyzed thicknesses are presented. As observed previously, the attenuation decreases as the attenuator thickness increases. For the *R1* configuration, the attenuation was 69.4%, while *R2* attenuated by 54.1%, and *R3* showed an attenuation of 46.2%. These differences are related to the material deformation: as the attenuator thickness increases, there is a greater loss of flow attenuation capacity. This loss occurs because the elastomeric material exhibits greater resistance to deformation, resulting in a decrease in the cumulative effect of the attenuator. To investigate this effect, deformations along the length of the attenuator were compared (Fig. 3b).

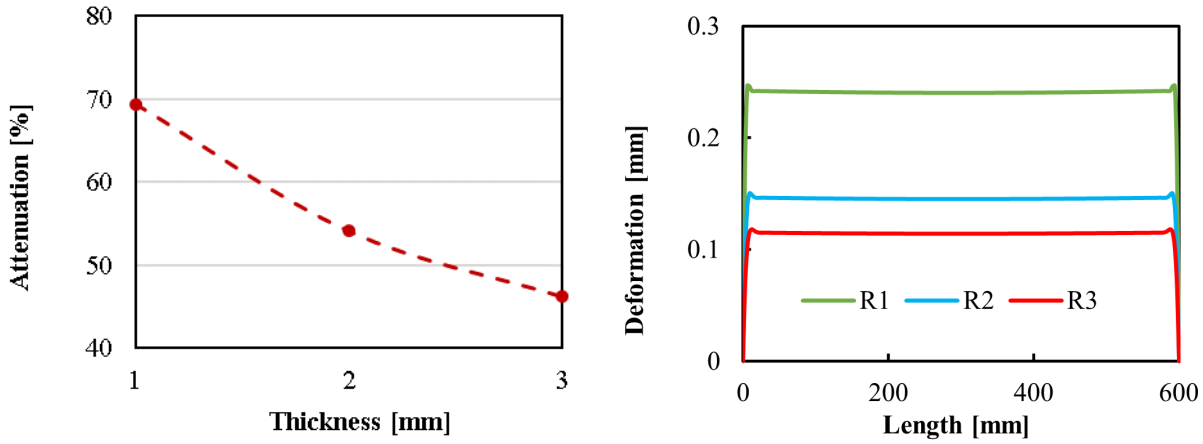

(a) Attenuation efficiency. (b) Deformations.

Figure 3: Attenuation efficiency and comparison between deformations for the reference attenuator and thickness along its length, for R1, R2 and R3.

The results in Figure 3b visually demonstrate a similar proportion to the attenuation values observed in Figure 3a. Thus, the thicker the elastomeric material, the greater the structural resistance, resulting in less deformation of the attenuator. In other words, less fluid is accumulated and returned to the system. Considering this behaviour is important in the design of the attenuator for applications that require a specific level of attenuation.

3.2 Influence of flow attenuator fractioning

Figure 4 depicts the outlet velocity of the reference attenuator (1 mm thick) split into 2 sections. It was observed that each section contributes to the total flow attenuation. When calculating the total attenuation based on the outlet velocity of section *B*, a value of 69.16% was obtained. It is essential to highlight that section *A* had a more substantial contribution to the reduction in outlet velocity, accounting for approximately 56.5% of the total attenuation, while section *B* contributed with 43.5%, in accordance with the results described by (Xiaohui *et al.*, 2015), which emphasize the importance of the location and order of attenuators in system performance. Therefore, section *A* initially received a higher proportion of the pulsating flow, resulting in a more significant contribution.

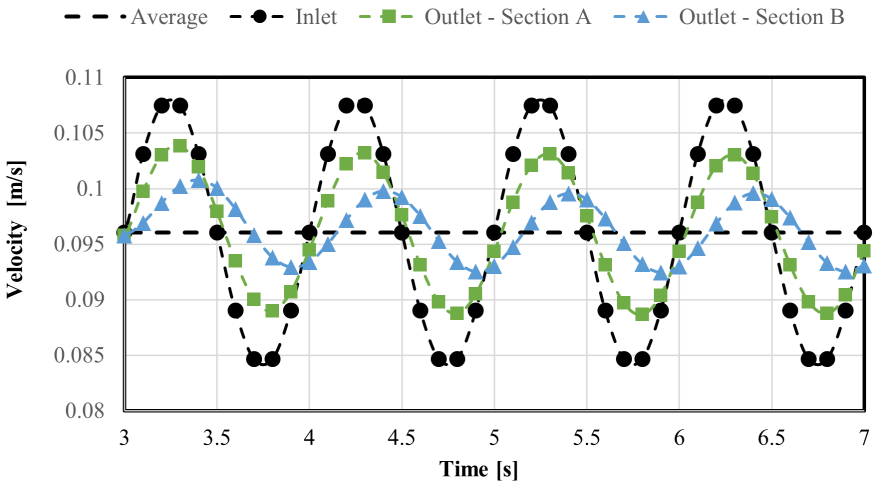

Figure 4: Comparison between inlet and outlet velocities for the reference attenuator fractionated into 2 sections (*R2S*). Sections *A* and *B* represent the 1st and 2nd sections, respectively, in the order of positioning.

The same analysis was performed for the fractionation of the reference attenuator into 3 sections (*R3S*) to investigate its effect on the attenuation efficiency (Figure 5). The total attenuation was 68.8%. Similarly, the most significant decreases in flow occurred in the order of positioning of the sections, with section *A* (37.4%) contributing more than section *B* (36.9%), which, in turn, contributed more than section *C* (25.7%). It is interesting to note that despite the differences in the contribution of each section, there is a relationship between this contribution and the number of sections. For example, in the *R2S* configuration, the distribution of attenuation is close to 1/2, while for the *R3S* configuration, it is close to 1/3

of the total attenuation. Therefore, this result indicates that the distribution of pulsating flow among the sections becomes more uniform as the attenuator is subdivided into a greater number of parts.

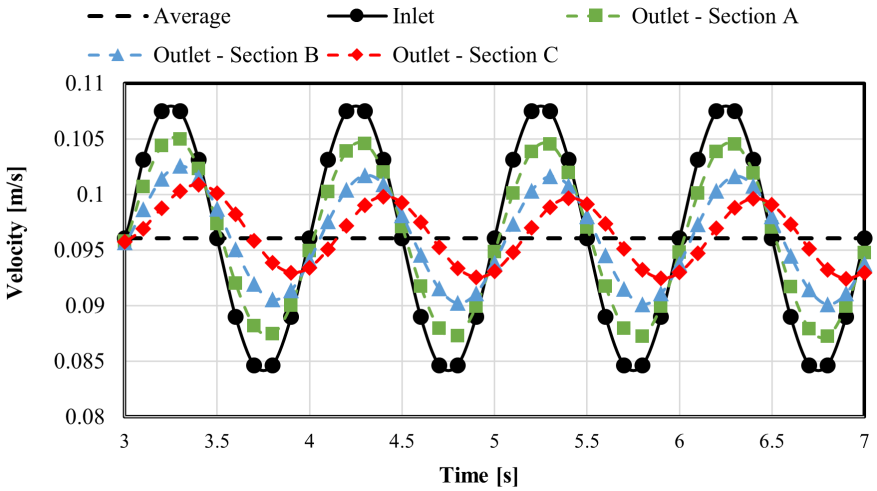

Figure 5: Comparison between the inlet and outlet velocities for the reference attenuator fractionated into 3 sections (R3S). Sections A, B, and C represent the 1st, 2nd, and 3rd sections, respectively, in the order of positioning.

Figure 6 presents the total attenuations for different configurations, including the reference *R1*, *R2S*, *R3S*, and *R10S* (reference fractionated into 10 sections). The *R10S* configuration was evaluated to analyze the attenuation behavior with a larger number of sections. It can be observed that the total attenuation values for *R2S* (69.16%), *R3S* (68.76%), and *R10S* (67.78%) are progressively lower compared to the reference configuration *R1* (69.41%). This trend is consistent with the quantitative analysis of the results, demonstrating that increasing the number of sections results in a slight decrease in the ability to attenuate pulsating flow. However, despite the reduction in the flow attenuation capacity with fractionation, this decrease is relatively insignificant, less than 0.5% for each fractionation performed. Thus, the use of fractionated attenuators can be advantageous in specific scenarios, such as in systems that require greater flexibility for adjustments.

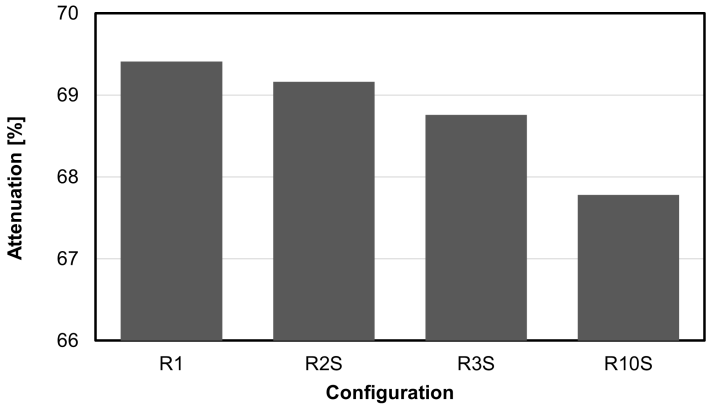

Figure 6: Efficiency of attenuation for the attenuators with the configurations R1, R2S, R3S, and R10S.

At this point, several factors can be considered as influencers of the attenuation reduction behavior concerning fractionation. The first factor is related to the type of fluid being transported and the dimensions of the attenuator device. The flow resistance is directly linked to the fluid's dynamic viscosity and the length of the tube, while inversely proportional to the fourth power of its radius. In the specific case of fractionation, only the length is modified, while the other parameters remain equally distributed. Consequently, the total resistance remains unchanged, as also noted by Dutra et al. (1999), since, for attenuators in series, the total resistance is equivalent to the sum of all individual resistances. Another factor is related to compliance, meaning the flexibility of the tube and the pressure acting inside the attenuator. Due to fractionation, there is a reduction in the internal area, resulting in an increase in force on its inner surface and, consequently, greater deformation in the attenuator. In other words, despite the decrease in length, the deformation remains the same when compared to the reference geometry, maintaining the total volume of accumulated fluid in each section. The effect of deformation concerning length can be visualized in Figure 7.

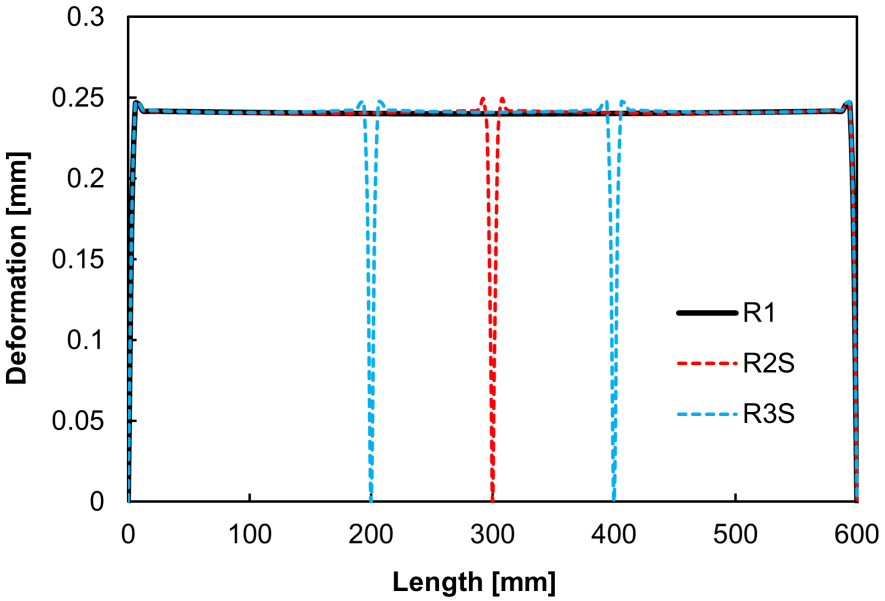

Figure 7: Comparison of deformation as a function of length for the geometries *R1*, *R2S*, and *R3S*.

In Figure 7, the regions where the attenuator is divided are highlighted. In this context, it can be observed that due to the presence of fixed supports, there is a loss in the accumulated volume. When considering a non-fractionated attenuator, only two supports are used. However, as the attenuator undergoes the fractionation process, there is a progressive utilization of a greater number of fixed supports.

3.3 Combined effect of thickness and fractionation

To evaluate the combined effect of thickness and fractionation of the attenuator, the thickness variation was simulated for the *R3S* configuration, at 1, 2, and 3 mm. The obtained results are presented in Figure 8, relating the thicknesses and sections (A, B, and C) to attenuation. Through it, it is possible to analyze the attenuation of each section separately for different thicknesses. It is observed that for section A with 1 mm thickness, there was an attenuation of 26.43%, for 2 mm, 20.88%, and for 3 mm, 17.88%, with percentage differences of 5.56% and 3%, but when it comes to sections B and C, these differences increase. These results suggest that the gradual increase in attenuator thickness is associated with a decrease in the slope of the attenuation curve. This is due to the fact that a portion of the loss is attributed to the fractionation process of the attenuator, with the highest attenuation capacity being observed in the initial sections.

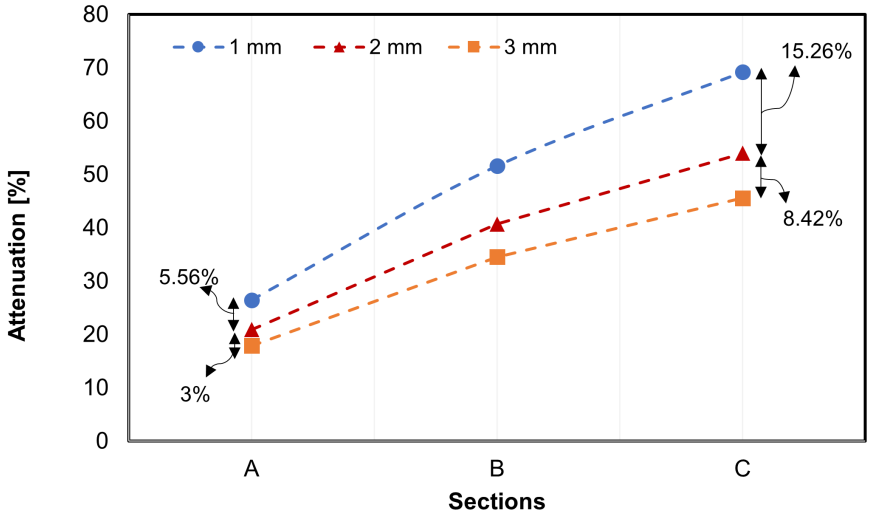

Figure 8: The combined effect of thickness on the attenuator divided into 3 sections (A, B, and C) on cumulative attenuation.

It was observed that there is a proportional difference in attenuation between the sections, regardless of the thickness of the attenuator. This means that each section contributes proportionally to the total attenuation of the flow. We can

understand this concept through Tab. 1, where the relative attenuations of each section are presented.

Table 1: Percentage of attenuation from the sections in relation to the total attenuation.

Sections	A	B	C
Attenuator thickness	Relative percentage		
1 mm	38.2%	36.4%	25.4%
2 mm	38.7%	36.7%	24.6%
3 mm	39.3%	36.5%	24.2%

4. CONCLUSION

The behavior of flow attenuating devices in pulsed flow was investigated numerically, analyzing the influence of their thickness on energy absorption and attenuation of flow peaks. The fractionation of the attenuators was also evaluated. and its effects on this configuration. The results showed that the thickness of the flux attenuator affects its ability to absorb energy. An increase in thickness results in lower outflow amplitude and reduced pulse attenuation. flow rates. Splitting the attenuator into sections contributes to attenuation total flow. Each section contributed to the reduction of the output speed, with the first section the most intense. As the number of sections increased, there were a more even distribution of the pulsating flow between them. However, the increase fractionation resulted in a slight decrease in the attenuation capacity of the pulsating flow due to loss of volume caused by fixed supports. When considering the thickness variation in fractional configurations, discrepancies were observed in flow attenuation. As the thickness increases, there is a difference percentage in the attenuation of each section, emphasizing the importance of taking into account both the thickness and fractionation of the attenuator when designing systems with specific levels of attenuation. This work has limitations and recommendations for future research. It is interesting to investigate the influence of the oscillation frequency tion of flow pulsations on attenuator performance. consider different frequencies allow evaluating the attenuation capacity of each attenuator section fractionated under different operating conditions. In addition, it is recommended to analyze separately the thickness of each fractional attenuator section to understand better the relationship between the thickness of the attenuator and the order of its placement for the case of series connection. Finally, it would be advantageous to carry out experiments practical tools to validate and improve the results obtained, since the simulations were conducted based on numerical models and simplified considerations.

5. REFERENCES

Bernart, V., 1999. "Pulsation dampening in suction and discharge systems for pd pumps". *World Pumps*, Vol. 1999, No. 397, pp. 20–24. ISSN 0262-1762. doi:https://doi.org/10.1016/S0262-1762(99)81400-X.

Hibbeler, R.C., 2016. *Mecânica dos Fluidos*. Pearson Education do Brasil, São Paulo, 1st edition. ISBN 978-85-430-1626-9. Título original: Fluid mechanics.

Sang, h., Ngo, L., Muhammad, S., Jeon, B. and Choi, H., 2017. "A comparative study between partitioned and monolithic methods for the problems with 3d fluid-structure interaction of blood vessels". *Journal of Mechanical Science and Technology*, Vol. 31, pp. 281–287. doi:10.1007/s12206-016-1230-2.

Shahzad, M., Kamran, A., Siddiqui, M.Z. and Farhan, M., 2015. "Mechanical characterization and fe modelling of a hyperelastic material". *Materials Research*, Vol. 18. doi:10.1590/1516-1439.320414.

Tey, W.Y., Asako, Y., Che Sidik, N.A., Che Sidik, N.A., Rui-Zher, G., Malaysia, U. and Lumpur, K., 2017. "Governing equations in computational fluid dynamics: Derivations and a recent review". Vol. 1, pp. 1–19.

Versteeg, H.K. and Malalasekera, W., 2007. *An Introduction to Computational Fluid Dynamics: The Finite Volume Method*. Pearson Education Limited, England, 2nd edition. ISBN 978-0-13-127498-3.

Viersma, T., 1980. *Analysis and Design of Hydraulic Servosystems and Pipelines*. Elsevier Scientific Publishing Company, Amsterdam.

Wang, W. and Yan, Y., 2010. "Strongly coupling of partitioned fluid–solid interaction solvers using reduced-order models". *Applied Mathematical Modelling*, Vol. 34, No. 12, pp. 3817–3830. ISSN 0307-904X. doi:https://doi.org/10.1016/j.apm.2010.03.022. URL `https://www.sciencedirect.com/science/article/pii/S0307904X10001381`.

Xiaohui, L., Shuping, C., Weijie, S. and et al., 2015. "Analysis and design of a water pump with accumulators absorbing pressure pulsation in high-velocity water-jet propulsion system". *Journal of Marine Science and Technology*, Vol. 20, No. 3, pp. 551–558. ISSN 1437-8213. doi:10.1007/s00773-015-0311-8.

6. RESPONSIBILITY NOTICE

The authors are solely responsible for the printed material included in this paper.